
Article:

Lupan, O, Santos-Carballal, D orcid.org/0000-0002-3199-9588, Magariu, N et al. (10 more authors) (2022) Al2O3/ZnO Heterostructure-Based Sensors for Volatile Organic Compounds in Safety Applications. ACS Applied Materials and Interfaces, 14 (25). pp. 29331-29344. ISSN 1944-8244

https://doi.org/10.1021/acsami.2c03704

Supporting Information

Al_2O_3/ZnO Heterostructure-Based Sensors for Volatile Organic Compounds in Safety Applications

Oleg Lupan,[1,2,3,*] David Santos-Carballal,[4,*] Nicolae Magariu,[2] Abhishek Kumar Mishra,[5] Nicolai Ababii,[2] Helge Krüger,[1] Niklas Wolff,[6] Alexander Vahl,[7,*] Mani Teja Bodduluri,[8] Niklas Kohlmann,[6] Lorenz Kienle,[6,*] Rainer Adelung,[1,*] Nora H de Leeuw,[4,9] Sandra Hansen,[1,*]

[1] *Department of Materials Science, Chair for Functional Nanomaterials, Faculty of Engineering, Christian-Albrechts Universität zu Kiel, Kiel, Kaiserstraße 2, D-24143 Kiel, Germany*
[2] *Center for Nanotechnology and Nanosensors, Department of Microelectronics and Biomedical Engineering, Faculty of Computers, Informatics and Microelectronics, Technical University of Moldova, 168 Stefan cel Mare str., MD-2004, Chisinau, Republic of Moldova*
[3] *Department of Physics, University of Central Florida, Orlando, Florida, FL 32816-2385, USA*
[4] *School of Chemistry, University of Leeds, Leeds LS2 9JT, United Kingdom*
[5] *Department of Physics, School of Engineering, University of Petroleum and Energy Studies (UPES), Energy Acres Building, Bidholi, Dehradun 248007, Uttrakhand, India*
[6] *Department of Materials Science, Chair for Synthesis and Real Structure, Faculty of Engineering, Christian-Albrechts Universität zu Kiel, Kiel, Kaiserstraße 2, D-24143 Kiel, Germany*
[7] *Department of Materials Science, Chair for Multicomponent Materials, Faculty of Engineering, Christian-Albrechts Universität zu Kiel, Kiel, Kaiserstraße 2, D-24143 Kiel, Germany*
[8] *Fraunhofer Institute for Silicon Technology (ISIT), Itzehoe, Fraunhoferstraße 1, D- 25524, Germany*
[9] *Department of Earth Sciences, Utrecht University, Princetonlaan 8a, 3584 CB Utrecht, The Netherlands*

[*] Corresponding authors:
Prof. Dr. O. Lupan, (ollu@tf.uni-kiel.de ; oleg.lupan@mib.utm.md)
Kiel University, Germany; Technical University of Moldova, Moldova; UCF, U.S.A.

Dr. David Santos-Carballal (d.santos-carballal@leeds.ac.uk)
University of Leeds, United Kingdom.

Prof. Dr. L. Kienle, (lk@tf.uni-kiel.de)
Kiel University, Germany

Prof. Dr. R. Adelung, (ra@tf.uni-kiel.de)
Kiel University, Germany

Dr. A. Vahl, (alva@tf.uni-kiel.de)
Kiel University, Germany

Dr. S. Hansen, (sn@tf.uni-kiel.de)
Kiel University, Germany

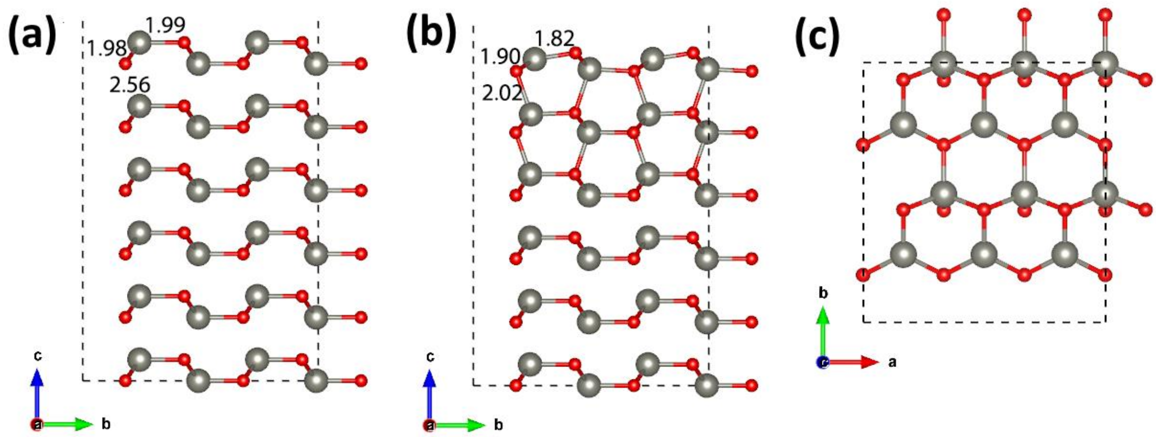

Figure S1. 2x2 supercell of the ZnO $(10\overline{1}0)$ surface: (a) side view of un-relaxed structure; (b) side view of relaxed structure; and (c) top view of relaxed structure.

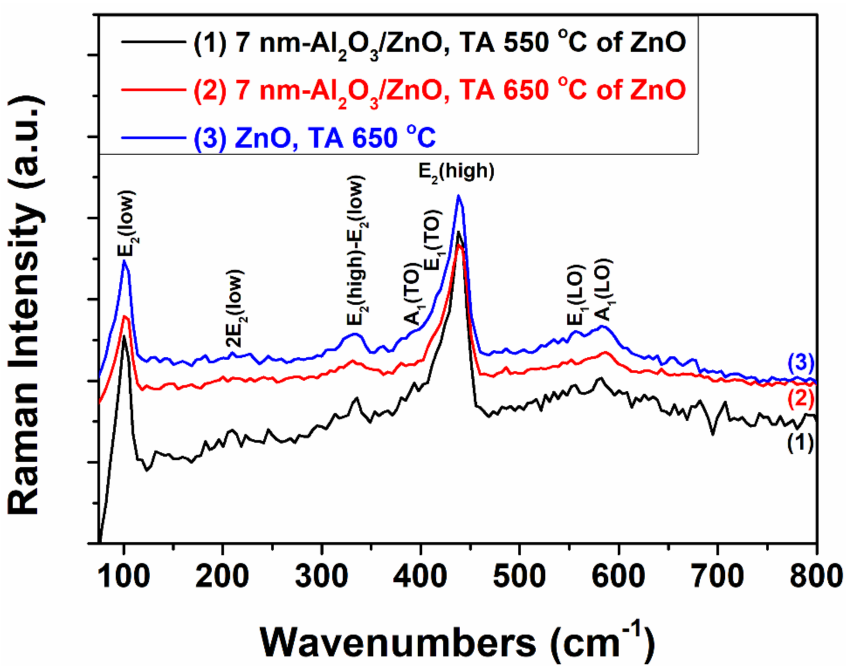

Figure S2. Micro-Raman spectra of the Al_2O_3/ZnO heterostructures after thermal annealing of the ZnO underlayer at 550 °C (curve 1) and 650 °C (curve 2) followed by thermal annealing at 620 °C for 40 min of the Al_2O_3 nano overlayer with a thickness of 7 nm. Micro-Raman spectrum of the ZnO after thermal annealing 650 °C (curve 3).

Supporting Information Text S1

Interestingly, no signal corresponding to Na (**Figure 5a**) was observed for the ZnO and ZnO/Al_2O_3 thin films grown over the quartz glass substrate, in contrast to all the thin film samples grown on the conventional glass slides. Thus, the use of quartz glass was a suitable method for the preparation of high purity ZnO and ZnO/Al_2O_3 thin films, which is especially required for device application.

The analysis of the XPS spectra of the Al_2O_3/ZnO heterostructures grown on the glass substrate shows the presence of the elements Na, O, Zn, C and Al, where each observed peak corresponds to each of these elements, see **Figure S3a**. The signal corresponding to C originates from atmospheric carbon compounds accumulating on the sample surfaces. The signals of Zn and Al are caused by the Al_2O_3/ZnO thin film, whereas the signal corresponding to Na is related to the heat treatment and the substrate material, which results in diffusion of this ion to the thin film surface. Finally, the O signal is partially due to atmospheric impurities and partially due to the Na, Zn and Al oxides forming the hetero-layered thin film.

The high-resolution spectrum of the Al-2p lines, shown in **Figure S3b**, exhibits a main peak, which is located at around 73.6 eV, as well as a second peak centered at 75.3 eV. Due to the limitations of the XPS setup used in this study, it is not possible to resolve the peaks of Al-$2p_{3/2}$ and Al-$2p_{1/2}$, which appear overlapped in our spectrum. The main peak around 73.6 eV is in reasonable good agreement with Al^{3+} in Al_2O_3, which is usually measured between 73.7 and 74.8 eV [1,2]. However, the additional component, which is centred at around 75.3 eV, indicates the presence of Al-OH bonds, similar to $Al(OH)_3$, which are usually reported between 74.0 and 75.7 eV [1,2].

The proximity, as well as the low and high intensity of the Zn and O signals, respectively, explain the overlap between the peak of the Zn-$2p_{3/2}$ line (centred around 1022.3 eV) and the O-KL_1L_1 Auger peak (observed at 1015.3 eV). However, the Zn-$2p_{3/2}$ peak signal, which appears at around 1022.3 eV, agrees well with Zn^{2+} in ZnO, which is usually reported between 1021.4 and 1022.5 eV.

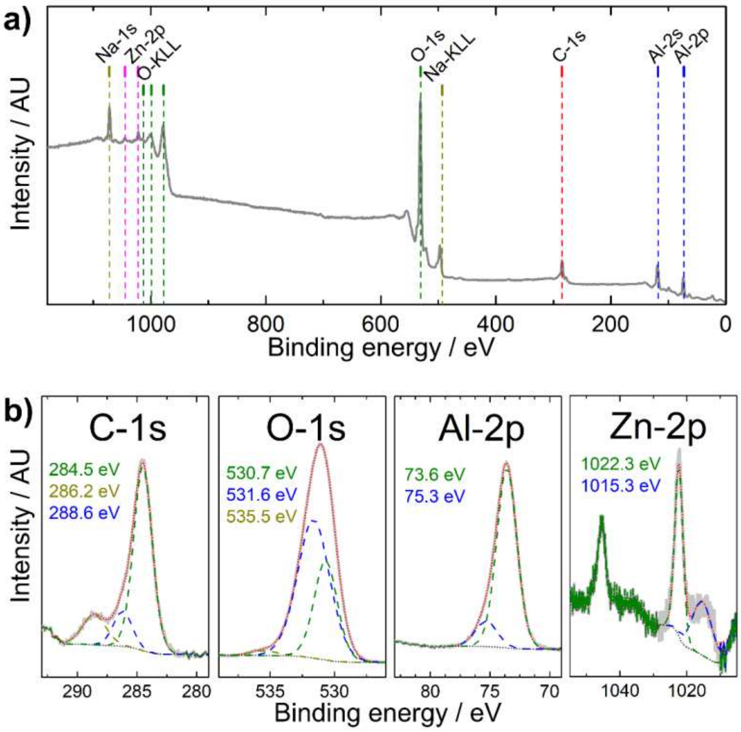

Figure S3. The analysis of the XPS spectra of the Al_2O_3/ZnO heterostructures deposited over glass substrates reveal the presence of the elements Na, Zn, O, Al and C, as shown by dashed lines in the survey spectrum (a). The peaks in the high-resolution spectra (b), corresponding to the C-1s, O-1s, Al-2p and Zn-2p lines, are fitted to several components (dashed lines), which positions are provided

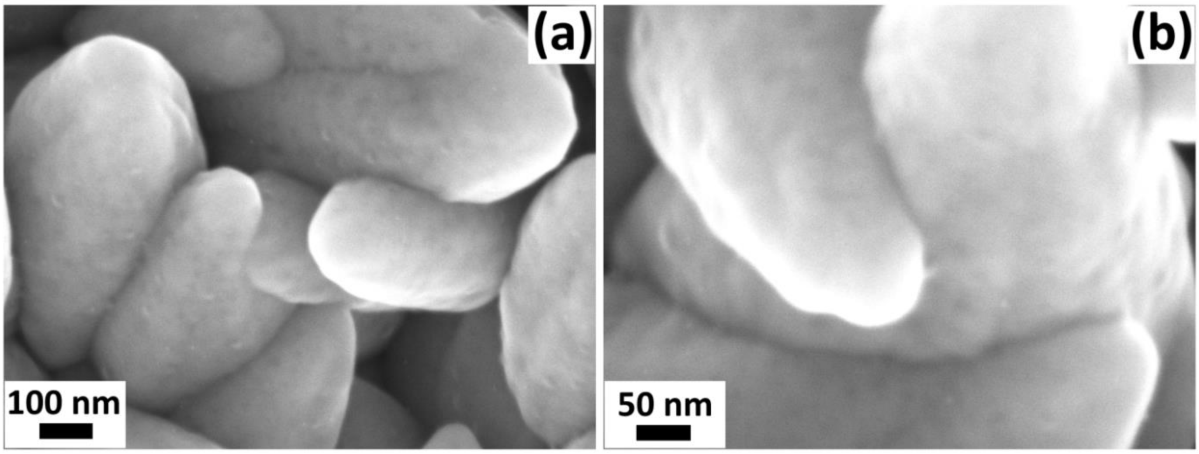

Figure S4. (a) SEM images at different magnifications, showing the intergrowth of the columar grains (b) of the freshly prepared columnar Al_2O_3/ZnO heterostructures coated with a nano-layer of 15 nm of thickness of Al_2O_3.

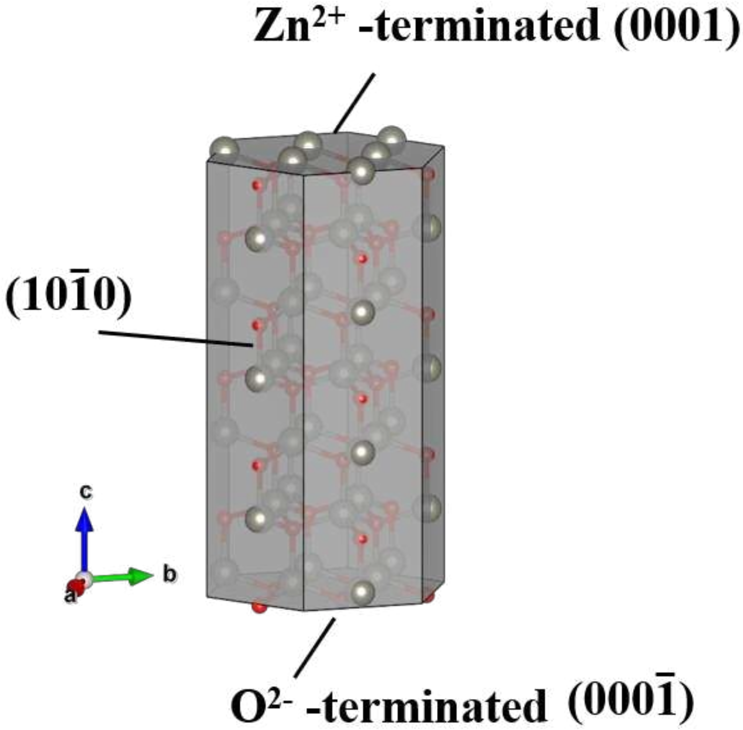

Figure S5. Crystallographic structure of ZnO showing the shape of a hexagonal prism and the Zn-terminated (0001), O-terminated $(000\bar{1})$ and $(10\bar{1}0)$ planes.

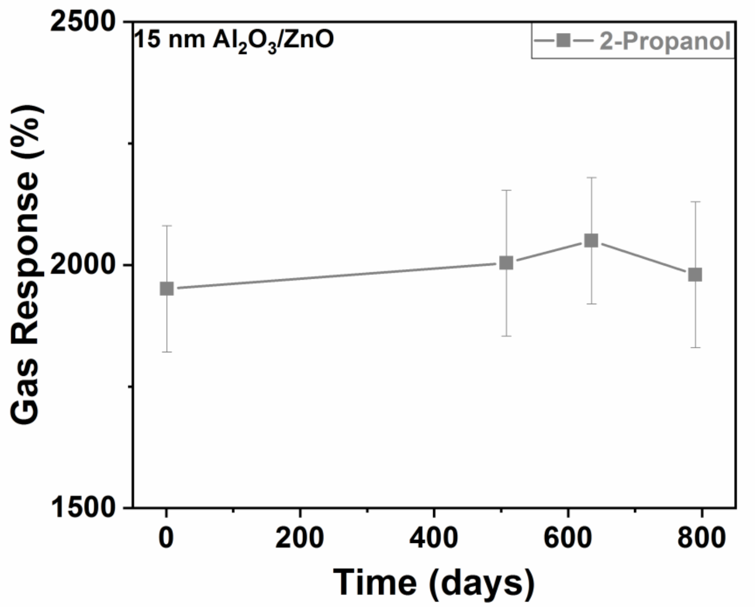

Figure S6. Variation of the gas response to 2-propanol vapors over time for the 15 nm-Al_2O_3/ZnO heterostructures.

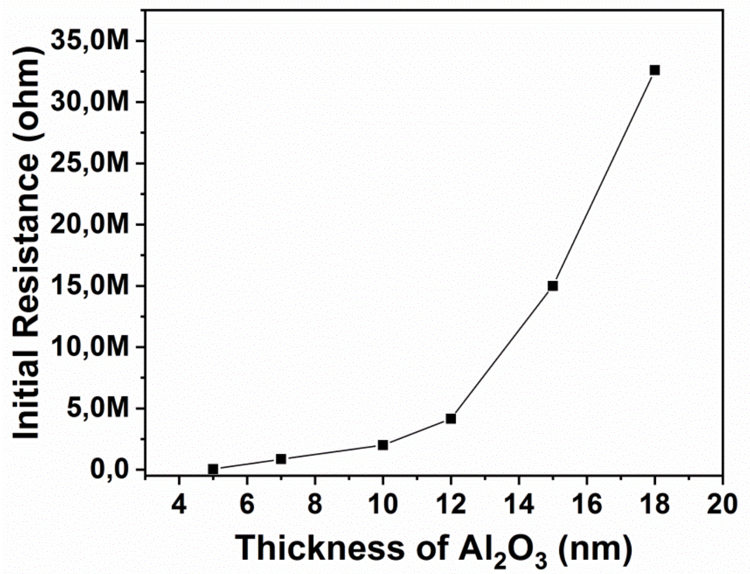

Figure S7. Initial electrical resistance of the Al_2O_3/ZnO heterostructure as a function of the thickness of the Al_2O_3 film.

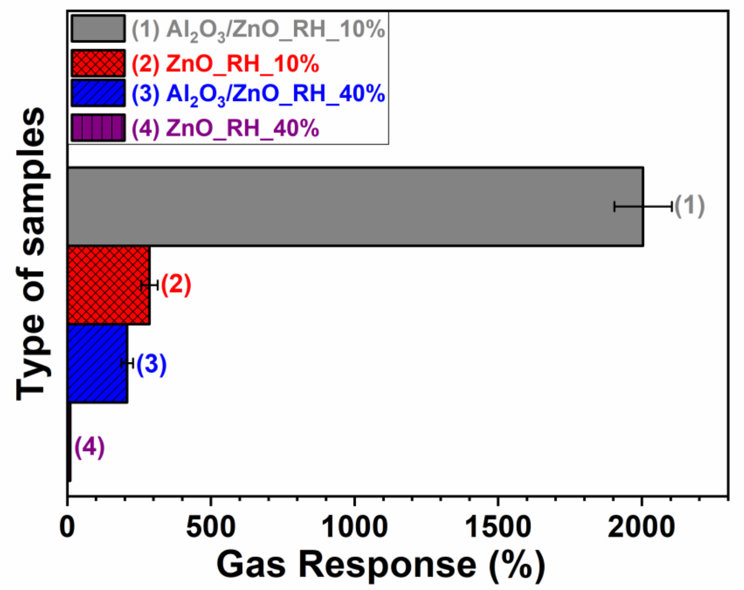

Figure S8. Influence of relative humidity on the response to 2-propanol of the ZnO films and Al_2O_3/ZnO heterostructures at different relative humidity values.

Table S1. Comparison of the reported 2-propanol sensors with large gas response values.

Individual structure	**2-Propanol conc. (ppm)**	**Gas response (Sensitivity) (R_{gas}/R_{air}), (R_{air}/R_{gas}) or (%)**	**Operating temperature (^oC)**	**Response time (s)**	**Recovery time (s)**	**Year of publication**
WO_3 Nanoplates [3]	200	4.31	250	70	115	2019
ZnO Nanotubes [4]	700	45	RT	450	550	2016
CuO [5]	300	24	300	13	247	2016
TiO_2 nanotube [6]	1000	36	RT	200	250	2014
Pd/TiO_2 nanorods [7]	5000	3.31	200	900	1020	2016
Al_2O_3/ZnO	**100**	**2000**	**350**	**30**	**50**	**Current work**

Supporting Information Text S2

Careful selection of the precursors used for the ALD deposition determines the type of n-n, n-p, p-n heterostructures that can be developed [8]. The new heterostructures prepared may offer an improved detection of gas, in comparison with the individual components of the sensor.[8]

The operation of a sensor is based in the detection of changes in the electrical conductivity of the material upon interaction with the gas. For n-type semiconductors, the variation of the thickness of the depletion layer is a typical parameter that can be used to control selectivity and sensitivity [9]. The applied VOC gases changes the conductivity of the material, since there are different oxygen species on the surface of the sensor, which affects the depletion layer [10,11,12].

Aluminum oxide (Al_2O_3), which is known for its excellent surface passivation properties [13], with a number of forbidden band lengths, depending on the particular metastable polymorph, including γ, η, δ, θ and χ [14]. Zou et al.[15] demonstrated that the amorphous aluminum oxide coating alters the conductivity of the mAl_2O_3/WO_3 composite heterostructure, which raises the number of catalytic reactions that take place on the surface, where oxygen species O^{2-}, O_2^- and O^- are adsorbed[15,16,17].

Previous reports [18,19] show that Al_2O_3 dissociates according to the following relation:

$$2Al_2O_3 \rightarrow 4Al^{3+} + 4O + O_2 + 12e^- \quad (1)$$

The Al_2O_3 and ZnO oxide phases of the heterostructure were deposited by combining the SCS approach with the ALD method respectively. The interface region or junction formed between these two semiconducting oxides plays an important role in the gas detection mechanism. The adsorption of atmospheric oxygen, on the surface of the heterojunction leads to a transfer of electrons from the conduction band to the different oxygen species (O_2^-, O^-, O^{2-}) formed at the surface [12]. Removing these oxygen species leads to the onset of spatial charge at the surface of the heterojunction. Exposing our heterostructures to the VOCs and inorganic gases trigger various surface reactions, leading to the dehydrogenation and the formation of various oxygen species. The commonly accepted [20] mechanism for the detection of gases and VOCs using zinc oxide

(ZnO)-based devices, involves adsorption and desorption reactions causing the formation of oxygen (O_2^-) following the extraction of an electron, e^-, from the semiconducting oxide. This process can be represented as follows [20]:

$$O_{2(\mathrm{gas})} + e^- \rightarrow O_{2(\mathrm{ads})} + e^- \rightarrow O^-_{2(\mathrm{ads})}. \quad (2)$$

The oxygen species $O_{(ads)}$ that form on the surface of zinc oxide when the sensor is exposed to air interact with the applied C_3H_8O vapor according to the relation [21]:

$$C_3H_8O + 9O^-_{(ads)} \rightarrow 4H_2O + 3CO_2 + 9e^- \quad (3)$$

We can see in equation (3) that the number of electrons increase in the accumulation layer after H_2O and CO_2 are formed, which also increases the electric current that can be detected by the heterostructure[22].

Al_2O_3 dissociates into Al^{3+}, oxygen species and free electrons, which catalyse efficiently the dehydrogenation reactions on the heterostructures surface and are responsible for the high response to 2-propanol gas, as mentioned by Zou et al. [15] .

Supporting Information Text S3

This work is the result of our continued efforts to develop new and improved gas sensors, especially based on columnar ZnO grown by the SCS approach. Pd-doped ZnO (ZnO:Pd) sensors were recently developed[23], where DFT calculations of the Pd-doped ZnO $< 10\bar{1}0 >$ surfaces showed good agreement with our experiments and provided an atomic level insight into the sensing mechanism. Eu-doped columnar ZnO films (ZnO:Eu) functionalized with Pd nanoparticles have also been explored for their gas sensing properties [24]. The simulation of the gas sensing mechanism of the ZnO:Eu$< 10\bar{1}0 >$ surfaces provided further understanding of the gas sensing mechanism, which is in excellent agreement with our recent works [23,25]. In the wurtzite-type structure, Zn and oxygen ions, which are coordinated by four oxygen and Zn ions, respectively, form individual planes of interconnected tetrahedra. The non-centrosymmetric wurtzite structure has two polar planes: the positively Zn^{2+} terminated (0001) plane and the negatively O^{2-} terminated $(000\bar{1})$ plane, as well as several non-polar planes, including the $(10\bar{1}0)$ surface [26,27,28,29] (see **Figure S5**). The non-polar $\{10\bar{1}0\}$ surfaces of ZnO have been under intensive investigation for gas sensing applications due to their high catalytic activity and microstructures, unlike the polar (0001) and $(000\bar{1})$ surfaces [30,31]. This supports our choice for using DFT methods for modeling the catalytic properties of the ZnO $(10\bar{1}0)$ surface [23,25,32,33] and to gain insight into the interaction of molecules with the columnar structures, whose surfaces are exposed to the test gas during the experiments. This study improves our atomic-level understanding of the surface reactions, by providing elemental information on the adsorption processes.

Supporting Information Text S4

The current-voltage (IV) behavior of a ZnO/Al_2O_3 heterostructure sensor with an Al_2O_3 layer thickness of 15 nm was characterized at different operating temperatures. The corresponding IV-curves are presented in **Figure S9**, as plots of the absolute current against the applied voltage. In general, the resistance of the heterostructure sensors decreases with increasing operating temperatures. For low operating temperatures, the heterostructure sensors exhibits a nearly linear IV characteristics with an ohmic resistance fitted to be around 15.9 MΩ at room temperature and 435 kΩ as well as 286 kΩ for operating temperatures of 150 and 200 °C, respectively. The fits are indicated by dashed lines in **Figure S9**. At operating temperatures above 200 °C, the IV characteristics become strongly nonlinear and deviate significantly from ohmic behavior. The observed temperature dependence of the I-V characteristics implies that additional conduction mechanisms become relevant at higher temperatures.

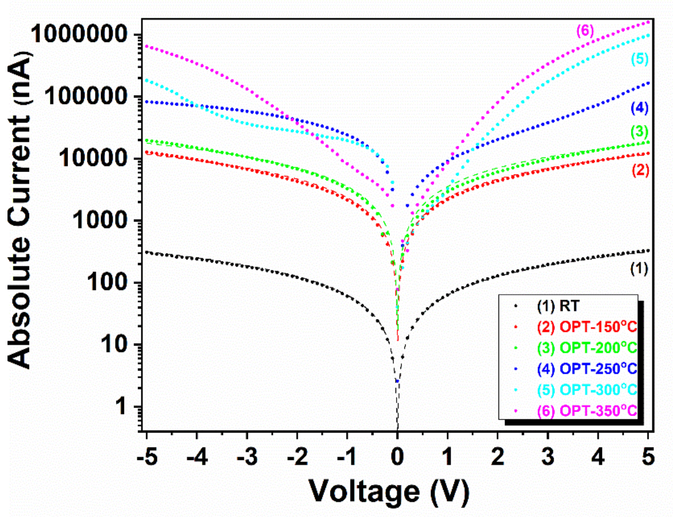

Figure S9. Current-Voltage characteristics of the ZnO/Al_2O_3 heterostructure sensor with an Al_2O_3 layer thickness of 15 nm at different operating temperatures, ranging from room temperature (black line), over 150 °C (red line), 200 °C (green line), 250 °C (blue line), 300 °C (cyan line), to 350 °C (magenta line).

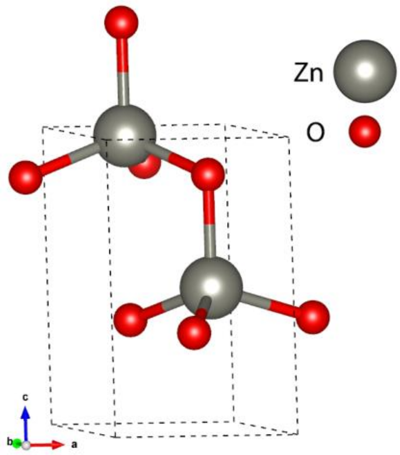

Figure S10. The unit cell of the ZnO wurtzite-type structure.

References

(1) Moulder, J. F.; Stickle, W. F.; Sobol, P. E.; Bomben, K. D. Handbook of X-Ray Photoelectron Spectroscopy; Perkin-Elmer Corporation: Eden Prairie, MN, 1992. *Google Sch. There is no Corresp. Rec. this Ref.* **1992**, 52–53.

(2) Naumkin, A. V; Kraust-Vass, A.; Gaarenstroom, S. W.; Powell, C. J. NIST X-ray Photoelectron Spectroscopy Database, National Institute of Standards and Technology. https://doi.org/10.18434/T4T88K.

(3) Acharyya, S.; Manna, B.; Nag, S.; Guha, P. K. WO_3 Nanoplates Based Chemiresistive Sensor Device for Selective Detection of 2-Propanol. In *2019 IEEE SENSORS*; IEEE, 2019; pp 1–4. https://doi.org/10.1109/SENSORS43011.2019.8956578.

(4) Acharyya, D.; Bhattacharyya, P. Alcohol Sensing Performance of ZnO Hexagonal Nanotubes at Low Temperatures: A Qualitative Understanding. *Sensors Actuators B Chem.* **2016**, *228*, 373–386. https://doi.org/10.1016/j.snb.2016.01.035.

(5) Ghosh, A.; Maity, A.; Banerjee, R.; Majumder, S. B. Volatile Organic Compound Sensing Using Copper Oxide Thin Films: Addressing the Cross Sensitivity Issue. *J. Alloys Compd.* **2017**, *692*, 108–118. https://doi.org/https://doi.org/10.1016/j.jallcom.2016.09.001.

(6) Hazra, A.; Dutta, K.; Bhowmik, B.; Chattopadhyay, P. P.; Bhattacharyya, P. Room Temperature Alcohol Sensing by Oxygen Vacancy Controlled TiO_2 Nanotube Array. *Appl. Phys. Lett.* **2014**, *105* (8), 081604. https://doi.org/10.1063/1.4894008.

(7) Şennik, E.; Alev, O.; Öztürk, Z. Z. The Effect of Pd on the H_2 and VOC Sensing Properties of TiO2 Nanorods. *Sensors Actuators B Chem.* **2016**, *229*, 692–700. https://doi.org/https://doi.org/10.1016/j.snb.2016.01.089.

(8) Marichy, C.; Pinna, N. Atomic Layer Deposition to Materials for Gas Sensing Applications. *Adv. Mater. Interfaces* **2016**, *3* (21), 1600335. https://doi.org/10.1002/admi.201600335.

(9) Zappa, D.; Galstyan, V.; Kaur, N.; Munasinghe Arachchige, H. M. M.; Sisman, O.; Comini, E. "Metal Oxide -Based Heterostructures for Gas Sensors"- A Review. *Anal. Chim. Acta* **2018**, *1039*, 1–23. https://doi.org/10.1016/j.aca.2018.09.020.

(10) Bhowmik, B.; Dutta, K.; Hazra, A.; Bhattacharyya, P. Low Temperature Acetone Detection by P-Type Nano-Titania Thin Film: Equivalent Circuit Model and Sensing Mechanism. *Solid. State. Electron.* **2014**, *99*, 84–92.

(11) Zhang, J.; Qin, Z.; Zeng, D.; Xie, C. Metal-Oxide-Semiconductor Based Gas Sensors: Screening, Preparation, and Integration. *Phys. Chem. Chem. Phys.* **2017**, *19* (9), 6313–6329. https://doi.org/10.1039/C6CP07799D.

(12) Mathew, M.; Shinde, P. V; Samal, R.; Rout, C. S. A Review on Mechanisms and Recent Developments in P-n Heterojunctions of 2D Materials for Gas Sensing Applications. *J. Mater. Sci.* **2021**, *56* (16), 9575–9604. https://doi.org/10.1007/s10853-021-05884-4.

(13) Ernst, M.; Walter, D.; Fell, A.; Lim, B.; Weber, K. Efficiency Potential of P-Type Al_2O_3/SiNx Passivated PERC Solar Cells With Locally Laser-Doped Rear Contacts. *IEEE J. Photovoltaics* **2016**, *6* (3), 624–631. https://doi.org/10.1109/JPHOTOV.2016.2535353.

(14) Levin, I.; Brandon, D. Metastable Alumina Polymorphs: Crystal Structures and Transition Sequences. *J. Am. Ceram. Soc.* **2005**, *81* (8), 1995–2012. https://doi.org/10.1111/j.1151-2916.1998.tb02581.x.

(15) Zou, Y.; Xi, S.; Bo, T.; Zhou, X.; Ma, J.; Yang, X.; Diao, C.; Deng, Y. Mesoporous Amorphous Al_2O_3 /Crystalline WO_3 Heterophase Hybrids for Electrocatalysis and Gas Sensing Applications. *J. Mater. Chem. A* **2019**, *7* (38), 21874–21883. https://doi.org/10.1039/C9TA08633A.

(16) Zhu, Y.; Zhao, Y.; Ma, J.; Cheng, X.; Xie, J.; Xu, P.; Liu, H.; Liu, H.; Zhang, H.; Wu, M.; Elzatahry, A. A.; Alghamdi, A.; Deng, Y.; Zhao, D. Mesoporous Tungsten Oxides with Crystalline Framework for Highly Sensitive and Selective Detection of Foodborne Pathogens. *J. Am. Chem. Soc.* **2017**, *139* (30), 10365–10373. https://doi.org/10.1021/jacs.7b04221.

(17) Raza, M. H.; Kaur, N.; Comini, E.; Pinna, N. SnO_2 -SiO_2 1D Core-Shell Nanowires Heterostructures for Selective Hydrogen Sensing. *Adv. Mater. Interfaces* **2021**, *8* (17), 2100939. https://doi.org/10.1002/admi.202100939.

(18) Patil, D. R.; Patil, L. A.; Amalnerkar, D. P. Ethanol Gas Sensing Properties of Al_2O_3-Doped ZnO Thick Film Resistors. *Bull. Mater. Sci.* **2007**, *30* (6), 553–559. https://doi.org/10.1007/s12034-007-0086-6.

(19) Kwon, C. H.; Hong, H.-K.; Yun, D. H.; Lee, K.; Kim, S.-T.; Roh, Y.-H.; Lee, B.-H. Thick-Film Zinc-Oxide Gas Sensor for the Control of Lean Air-to-Fuel Ratio in Domestic Combustion Systems. *Sensors Actuators B Chem.* **1995**, *25* (1–3), 610–613. https://doi.org/10.1016/0925-4005(95)85134-8.

(20) Mishra, Y. K.; Modi, G.; Cretu, V.; Postica, V.; Lupan, O.; Reimer, T.; Paulowicz, I.; Hrkac, V.; Benecke, W.; Kienle, L.; Adelung, R. Direct Growth of Freestanding ZnO Tetrapod Networks for Multifunctional Applications in Photocatalysis, UV Photodetection, and Gas Sensing. *ACS Appl. Mater. Interfaces* **2015**, *7* (26), 14303–14316. https://doi.org/10.1021/acsami.5b02816.

(21) Luo, Y.; Ly, A.; Lahem, D.; Zhang, C.; Debliquy, M. A Novel Low-Concentration Isopropanol Gas Sensor Based on Fe-Doped ZnO Nanoneedles and Its Gas Sensing Mechanism. *J. Mater. Sci.* **2021**, *56* (4), 3230–3245. https://doi.org/10.1007/s10853-020-05453-1.

(22) Hoppe, M.; Lupan, O.; Postica, V.; Wolff, N.; Duppel, V.; Kienle, L.; Tiginyanu, I.; Adelung, R. $ZnAl_2O_4$ -Functionalized Zinc Oxide Microstructures for Highly Selective Hydrogen Gas Sensing Applications. *Phys. status solidi* **2018**, *215* (7), 1700772. https://doi.org/10.1002/pssa.201700772.

(23) Lupan, O.; Postica, V.; Adelung, R.; Labat, F.; Ciofini, I.; Schürmann, U.; Kienle, L.; Chow, L.; Viana, B.; Pauporté, T. Functionalized Pd/ZnO Nanowires for Nanosensors. *Phys. status solidi - Rapid Res. Lett.* **2018**, *12* (1), 1700321. https://doi.org/10.1002/pssr.201700321.

(24) Lupan, C.; Khaledialidusti, R.; Mishra, A. K.; Postica, V.; Terasa, M. I.; Magariu, N.; Pauporté, T.; Viana, B.; Drewes, J.; Vahl, A.; Faupel, F.; Adelung, R. Pd-Functionalized ZnO:Eu Columnar Films for Room-Temperature Hydrogen Gas Sensing: A Combined Experimental and Computational Approach. *ACS Appl. Mater. Interfaces* **2020**, *12* (22),

24951–24964. https://doi.org/10.1021/acsami.0c02103.

(25) Lupan, O.; Magariu, N.; Khaledialidusti, R.; Mishra, A. K.; Hansen, S.; Krüger, H.; Postica, V.; Heinrich, H.; Viana, B.; Ono, L. K.; Cuenya, B. R.; Chow, L.; Adelung, R.; Pauporté, T. Comparison of Thermal Annealing versus Hydrothermal Treatment Effects on the Detection Performances of ZnO Nanowires. *ACS Appl. Mater. Interfaces* **2021**, *13* (8), 10537–10552. https://doi.org/10.1021/acsami.0c19170.

(26) Kamble, A. S.; Sinha, B. B.; Chung, K.; Gil, M. G.; Burungale, V.; Park, C.-J.; Kim, J. H.; Patil, P. S. Effect of Hydroxide Anion Generating Agents on Growth and Properties of ZnO Nanorod Arrays. *Electrochim. Acta* **2014**, *149*, 386–393. https://doi.org/10.1016/j.electacta.2014.10.049.

(27) Adegoke, K. A.; Iqbal, M.; Louis, H.; Jan, S. U.; Anam, M.; Bello, O. S. Photocatalytic Conversion of CO2Using ZnOSemiconductor by Hydrothermal Method. *Pakistan J. Anal. Environ. Chem.* **2018**, *19* (1), 1–27. https://doi.org/10.21743/pjaec/2018.06.01.

(28) Hancock, J. M.; Rankin, W. M.; Woolsey, B.; Turley, R. S.; Harrison, R. G. Controlled Formation of ZnO Hexagonal Prisms Using Ethanolamines and Water. *J. Sol-Gel Sci. Technol.* **2017**, *84* (1), 214–221. https://doi.org/10.1007/s10971-017-4486-9.

(29) Kohlmann, N.; Hansen, L.; Lupan, C.; Schürmann, U.; Reimers, A.; Schütt, F.; Adelung, R.; Kersten, H.; Kienle, L. Fabrication of ZnO Nanobrushes by H_2–C_2H_2 Plasma Etching for H_2 Sensing Applications. *ACS Appl. Mater. Interfaces* **2021**, *13* (51), 61758–61769. https://doi.org/10.1021/acsami.1c18679.

(30) Patolsky, F.; Timko, B. P.; Zheng, G.; Lieber, C. M. Nanowire-Based Nanoelectronic Devices in the Life Sciences. *MRS Bull.* **2007**, *32* (2), 142–149. https://doi.org/10.1557/mrs2007.47.

(31) Pan, Z. W.; Dai, Z. R.; Wang, Z. L. Nanobelts of Semiconducting Oxides. *Science (80-.).* **2001**, *291* (5510), 1947–1949. https://doi.org/10.1126/science.1058120.

(32) Prades, J. D.; Cirera, A.; Morante, J. R. Ab Initio Calculations of NO_2 and SO_2 Chemisorption onto Non-Polar ZnO Surfaces. *Sensors Actuators B Chem.* **2009**, *142* (1), 179–184. https://doi.org/10.1016/j.snb.2009.08.017.

(33) Chen, D.; Zhang, X.; Tang, J.; Cui, H.; Pi, S.; Cui, Z. Adsorption of SF6 Decomposed Products over ZnO($10\bar{1}0$): Effects of O and Zn Vacancies. *ACS Omega* **2018**, *3* (12), 18739–18752. https://doi.org/10.1021/acsomega.8b02933.